# Ligand-Field Theory-Based Analysis of the Adsorption Properties of Ruthenium Nanoparticles

Iker del Rosal,[†] Maxime Mercy,[†,‡] Iann C. Gerber,[†] and Romuald Poteau[†,*]

[†]Université de Toulouse, INSA, UPS, CNRS, LPCNO (IRSAMC), 135 avenue de Rangueil, F-31077 Toulouse, France. [‡]Present address: Department of Chemistry, University College London, 20 Gordon Street, London WC1H 0AJ, United Kingdom.

ABSTRACT The experimental design of improved nanocatalysts is usually based on shape control and is surface-ligand dependent. First-principle calculations can guide their design, both in terms of activity and selectivity, provided that theoretical descriptors can be defined and used in a prescreening process. As a consequence of the Sabatier principle and of the Brønsted—Evans—Polanyi relationship, an important prerequisite before optimizing the catalytic properties of nanoparticles is the knowledge of the selective adsorption strengths
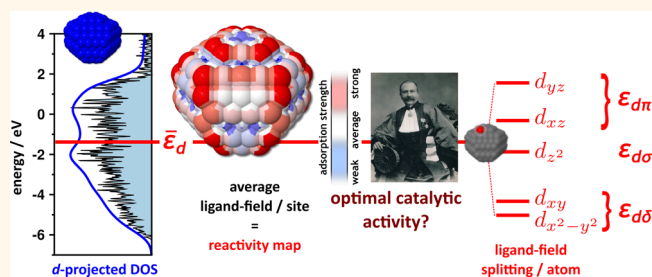
of reactants at their surface. We report here adsorption energies of X (H, CH_3) and L (PH_3, CO) ligands at the surface of bare ruthenium nanoclusters Ru_n ($n = 55$ and 147) calculated at the DFT level. Their dependence on the topology of the adsorption sites as well as on the size and shape of the nanoparticles (NPs) is rationalized with local descriptors derived from the so-called d-band center model. Defining the descriptors involves the determination of the energy of effective d atomic orbitals for each surface atom. Such a ligand field theory-like model is in close relation with frontier molecular orbital theory, a cornerstone of rational chemical synthesis. The descriptors are depicted as color maps which straightforwardly yield possible reactivity spots. The adsorption map of a large spherical hcp cluster (Ru_{288}) nicely confirms the remarkable activity of steps, the so-called B_5 sites. The predictive character of this conceptual DFT approach should apply to other transition metal NPs and it could be a useful guide to the design of efficient nanocatalysts bearing sites with a specific activity.

KEYWORDS: DFT · ruthenium · nanocatalysis · Sabatier principle · reactivity descriptors

Nanoparticles (NPs) exhibit physical and chemical properties intermediate between those of small molecular compounds and the bulk material, resulting from surface or quantum size effects.[1] Special sites[2] are also known to play a role in heterogeneous catalysis[3] and in synthesis over nanoparticles.[4,5] More efficient nanocatalysts need to be developed, yet the task of discovering novel alternatives has proven to be extremely challenging. We focus in the present paper on ruthenium NPs (RuNPs), revisiting some key concepts by means of first-principle DFT calculations. Ruthenium and its derivatives constitute an important class of catalysts, involved in hydrogenolysis reactions,[6] olefin metathesis,[7] hydrogenation of aromatic compounds,[8,9] and the Fischer—Tropsch reaction.[10,11] It is a catalyst of utmost importance which deserves a deeper understanding of its surface properties under the NP state, a range of sizes with possible quantum

size effects. With the surface properties being ruled by the intrinsic electronic structure of the metal NPs, quantum chemistry is expected to provide valuable insights and to guide the development of new catalysts. But is theoretical chemistry able to provide clues about the structure and reactivity of colloidal nanoparticles (NPs) as well as useful guidelines to experimentalists, regarding the complexity of such problems? Despite some recent spectacular results (see ref 12 and references therein), quantum chemistry is not mature enough to reach a *routine* understanding of the activity of nanoparticles similar to that gained on organometallic complexes in homogeneous catalysis[13] and to contribute to the rational design of nanocatalysts. State-of-the-art quantum chemistry studies of homogeneous and heterogeneous[14,15] processes involve the exploration of potential energy surfaces in order to elucidate multistep reaction paths. But complex reactions that occur at the surface of NPs

© 2013 American Chemical Society

have scarcely been investigated with such computational approaches.[16,17] The reason lies in the complexity and the diversity of the metal sites, and the presence of ancillary ligands and other surface species, which make such calculations difficult to achieve with current computational quantum chemistry tools. Theoretical chemists usually get around this problem by considering NPs as faceted crystals, *i.e.*, as a juxtaposition of flat, kinked and stepped surfaces. They can thus take advantage of periodic-boundary DFT methods to use chain-of-states based methods for finding minimum energy pathways.[18−20] On the other hand, it is also possible to consider metallic clusters as scale models of NPs, usually made of less than 100 metal atoms.[21−31] Both approaches share the same drawback: they do not consider the essence of NPs, *i.e.*, the fundamental question of quantum-size effects. The outrageous cost of the quantum chemistry exploration of reaction pathways as well as such finite-size effect challenges the *in silico* understanding and design of selective and catalytically efficient NPs.
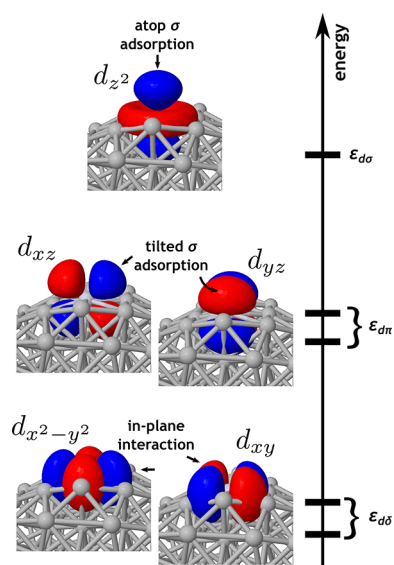
We propose to tackle this problem by developing DFT-based reactivity descriptors aiming at predicting the local activity of RuNPs. They are derived from the d-band center model of Hammer and Nørskov,[32,33] widely used for explaining trends in the catalytic activity of metal surfaces. Within this model, a d-band center parameter, ε_d, is computed as the normalized, energy-weighted integral of the density of states (DOS), projected onto all d atomic orbitals of the surface atoms involved in a given adsorption site. It is important to underline that the information contained in the DOS is reduced to a single energy level, making a connection with frontier orbital theory. Despite its simplicity, this monoelectronic descriptor has proved to be very powerful to explain trends in adsorption energies. A linear relationship between the center of the d-band and the binding energy of the adsorbate to the surface is often observed: the closer to the Fermi level, the stronger the adsorption energy. According to the Brønsted−Evans−Polanyi (BEP) relationship[34,35] and to the Sabatier principle of maximizing catalytic activity by optimizing the adsorption energy of reactants,[36−39] this has consequences well beyond the understanding of trends in adsorption energies. Indeed, the BEP equation relates the change in activation energy of a reaction to the change in the reaction energy: $\delta E_{act} = \alpha \delta E_r$. As a consequence, the catalytic activity of heterogeneous catalysts within the periodic table is well described by Balandin's volcano relations between reaction rates and adsorption energies.[38,40] It has been extensively and successfully used in the analysis of surface elementary steps of heterogeneous catalytic processes.[41−43] Note that this approach was used to guide the design of a new CoMo-based alloy catalyst for ammonia synthesis.[44] If we turn to the matter of selectivity at the surface of NPs, the activity

of a step or kink can also be inferred from the comparison of ε_d calculated by selecting appropriate surface atoms in different $\{hkl\}$ crystallographic planes.[3] Nonetheless, owing to the surface complexity of moderate size transition metal NPs and to the possible presence of defects and special sites, a model aiming at rationalizing adsorption properties at their surface should be able to go beyond the simple picture given by a d-band center average value, by taking into account the individual contributions of d atomic orbitals (AOs), as it is done in molecular inorganic chemistry. Another interesting approach aiming at generating *ab initio* quantitative descriptors of bond strengths in heterogeneous catalysts has also been proposed,[37,45] but it does not seem to be easily transferable to NPs. In a sense, the frontier orbital equation is more powerful, since a chemical interaction can be analyzed not only from energy levels of the interacting molecules, but also from the overlap between them, which serves as basis for understanding the selectivity observed in some reactions.[46] This is why we propose a new formulation of the d-band center model that goes beyond its original formulation by yielding a local electronic fingerprint of each surface site of a nanocatalyst.

We first check that the d-band center value calculated for all surface atoms of several Ru_n clusters, $\langle \varepsilon_d \rangle$, accounts for the simultaneous adsorption of H atoms. The local adsorption strength of hydrides at the surface of a Ru_{55} cluster is then analyzed and interpreted by an on-site d-band center descriptor (hereafter noted $\bar{\varepsilon}_d(\mu_k)$). It is depicted as a color map that gives a straightforward point of view of the expected adsorption strength at the surface of RuNPs. The predictive ability of this descriptor is then assessed by calculating the adsorption energy of CO, CH_3 and PH_3 ligands on various sites of Ru_n clusters ($n = 55, 147$). The apparent discrepancies are accounted for by introducing new descriptors that give an indication of the σ, π and δ affinities of adsorption sites. On the basis of a meticulous analysis of these results, we formulate the powerful idea to reduce the huge amount of information contained in the electronic structure of metal NPs to effective d orbitals for each metal atom of the surface (Scheme 1). Following these lines, an analysis of the electronic features of an hcp NP with realistic size (Ru_{288}) is provided. This analysis agrees with the well-known special site nature of steps in such ruthenium NPs. We finally conclude that our approach which combines both ligand-field theory and a related fragment molecular orbitals method may be a very useful way to identify the most active sites at the surface of a metal NP and we propose a conjecture related to the Sabatier principle.

MODEL AND RESULTS

The Original d-Band Center Model. A comprehensive model is needed to understand the DFT adsorption energies calculated in this study. It has been shown in

atop σ
adsorption

d_{z^2}

$\varepsilon_{d\sigma}$

d_{xz} tilted σ
adsorption d_{yz}

$\Big\}\ \varepsilon_{d\pi}$

$d_{x^2-y^2}$ in-plane
interaction d_{xy}

$\Big\}\ \varepsilon_{d\delta}$

energy

Scheme 1. Effective d AOs.

several studies that the adsorption strength of chemical species on metal surfaces can be understood in terms of Hammer and Nørskov's d-band center model.[32,33,47] It is not so different from Hoffmann's approach which is more straightforwardly related to frontier orbital theory.[48] Within this model, the interaction between an adsorbate and a surface is separated into two contributions. First, the adsorbate interacts with the transition metal sp states and then the contribution of d states is taken into account ($\Delta E = \Delta E_{sp} + \Delta E_d$). According to this model, ΔE_{sp} coupling can be considered to be essentially a constant. The main contribution to the variations in bond energy from one transition metal to the next comes from the coupling to the metal d states (ΔE_d). In a simplified description, the stabilization energy is given by a second-order perturbation theory term, $\Delta E_d = V^2/|\varepsilon_{ads} - \varepsilon_d|$, where V is the coupling element between the adsorbate state of energy ε_{ads} and the metal d states centered at ε_d. The d-band center, $\bar{\varepsilon}_d(\mu_k)$, is then computed as the normalized, energy-weighted integral of the density of states (DOS), projected onto *all* d atomic orbitals (AOs) of the surface atoms which characterize the μ_k coordination site:

$$\bar{\varepsilon}_d(\mu_k) = \frac{\left(\displaystyle\sum_{\alpha \in \mu_k} \sum_m \int_{E_{min}}^{E_{max}} \varepsilon n_{d_m}(\alpha, \varepsilon)\, d\varepsilon\right)}{\left(\displaystyle\sum_{\alpha \in \mu_k} \sum_m \int_{E_{min}}^{E_{max}} n_{d_m}(\alpha, \varepsilon)\, d\varepsilon\right)} \quad (1)$$

where m runs over the five d AOs and $n_{d_m}(\alpha,\varepsilon)$ is the atom-projected density of states on the d_m AO of atom α; μ_k is reminiscent of the symbol which designates bridging ligands in coordination chemistry and the bar sign above ε_d means that it is averaged over all d AOs.

Although E_{min} is readily set to the bottom of the occupied d-band, the d-band center cannot be defined unambiguously within a plane-wave approach. Following

a previous suggestion of Stroppa and Kresse,[49] we chose to calculate the center of gravity of the occupied d-band, *i.e.*, we integrated up to the Fermi level E_F, which is a lower bound for the d-band center usually calculated (see also a short discussion in the Supporting Information).

The interaction between an adsorbate and a metal surface is based on few parameters only, including the filling, average energy and width of the localized d-band of the metal surface, the adsorbate molecular orbital energies and the geometric overlap between the surface and adsorbate orbitals. We shall now recall a key point of frontier orbital theory, dealing with the adsorption of organic ligands on middle transition metal surfaces. In addition to the so-called two-electron, two-orbital stabilizing interactions, the four-electron, two-orbital interactions may be attractive, owing to the partial filling of the d-band. It turns out that this two-orbital, four-electron interaction, which is related to steric effects in orbital theory applied to molecules, may involve an additional stabilizing charge transfer from ligands to the surface. This interaction again becomes a destabilizing agent in the case of very late transition metal surfaces. With the stabilizing four-electron, two-orbital interaction partially involved in the adsorption of species on ruthenium surfaces, setting up the upper bound of the integral to the Fermi level makes sense. In addition, it is expected to capture the trends in case of a metal-to-ligand π^* backbonding.

But in its original formulation, the $\bar{\varepsilon}_d$ descriptor may not be powerful and accurate enough to account for selective processes that occur at the surface of NPs, since it is an average value. Yet, orbital interactions between metal atoms and ligands are ruled by the symmetry of the individual d AOs.[50] This is a strong limitation of the d-band center model and a conceptual difference with respect to molecular orbital theory.[51,52] Unfortunately, the intrinsic chemical properties at the surface of transition metal NPs do not lie within a few states around the Fermi level. This is why we propose a model that combines the powerful ligand-field theory with the reduction of the information contained in the projected DOS to a few effective energy levels, as shown in Scheme 1.

Optimal Coverage of Metal Surfaces by H Atoms. Here, we investigate the possible relationship between the average d-band center of surface atoms, $\langle\varepsilon_d\rangle$, and the dissociative adsorption energy of hydrides, $E_{ads}(H_2)$, on the surface of several Ru systems: the icosahedral Ru_{13}, four Ru_{55} clusters (icosahedron, IC; cuboctahedron, CB; Marks decahedron-like, MD; spherical piece of an hcp crystal, HCP) and the flat Ru(0001) surface. $\langle\varepsilon_d\rangle$ is calculated as:

$$\langle\varepsilon_d\rangle = \frac{\left(\displaystyle\sum_{\alpha \in surf} \int_{E_{min}}^{E_F} \varepsilon n_d(\alpha, \varepsilon)\, d\varepsilon\right)}{\left(\displaystyle\sum_{\alpha \in surf} \int_{E_{min}}^{E_F} \varepsilon n_d(\alpha, \varepsilon)\, d\varepsilon\right)} \quad (2)$$

Among the four Ru_{55} clusters, the HCP isomer is the most stable, whereas the IC isomer lies a few kcal/mol above (see Table S1). According to electron-count rules, naked Ru_n clusters can accommodate a large number of surface ligands. The expected linear relationship between $\langle \varepsilon_d \rangle$ and $E_{ads}(H_2)$ is observed for optimal coverage values, as a consequence of the balance between the stabilization of the metal core gained by the presence of surface species and the minimization of the steric hindrance between them. Several coverage values (τ) have been considered for each cluster, ranging approximately from $\tau = 0.25$ to $\tau = 2.0$, sometimes starting from different coordination of hydrides for the same τ value. The graph plot in Figure 1 confirms that the d-band center $\langle \varepsilon_d \rangle$ is a good indication of the adsorption strength at the surface of
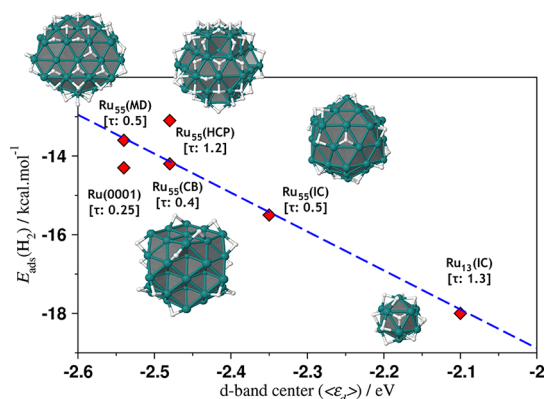

Figure 1. Plot of the average H_2 dissociative adsorption energy ($E_{ads}(H_2)$, in kcal/mol) as a function of the surface atoms average d-band center ($\langle \varepsilon_d \rangle$, in eV), where E_{ads} (H_2) = $(1/m)[E(Ru_nH_m) - E(Ru_n) - (m/2)E(H_2)]$. τ is the H:surface Ru coverage value.

nanoclusters. But the point we specifically want to address in this paper is to go beyond the seminal formulation of the d-band center model, by predicting the activity and selectivity of local sites at the surface of metal NPs. It is now going to be examined by calculating the dissociative adsorption energy of H_2 on several adsorption sites of the $Ru_{55}(MD)$ cluster.

On-Site Dependence of the Adsorption of H_2 on Ru_{55}. Beyond a certain size, it is experimentally known that RuNPs adopt a spherical hcp structure. It is the case of the 1 nm $Ru_{55}(MD)$ NP shown in Figure 1, chosen owing to the topological diversity of its surface. It has been adapted from the Cd_{55} cluster previously studied by Doye.[53] Although it has no overall order, strong structural preferences can be identified in this structure reminiscent of a Marks decahedron:[54,55] one side can be seen as two Ru(0001) surfaces with a bending angle of 154°, whereas on the opposite side two Ru atoms are low-coordinate, owing to the presence of a subsurface defect. This structural feature is interesting inasmuch as it shows what the electronic fingerprint of such a defect in RuNPs would be. Forty-one adsorption sites were systematically considered. A color scale was adopted in maps **A−C** (Figure 2a). It was set up according to $E_{ads}(H_2)$ calculated for the Ru(0001) plane (see ref 56 and references therein for a comparison with experimental values and other theoretical studies): white for $H*fcc$ (−13.6 kcal/mol), light blue for $H*hcp$ (−11.0 kcal/mol) and $H*bridge$ (−10.1 kcal/mol), and dark blue for $H*atop$ (−3.3 kcal/mol). Such color maps give a straightforward indication of the adsorption strength of H atoms on all the sites probed. Some interesting results can be extracted from these data: (i) H atoms adsorb on the atop, μ and μ_3 sites of the
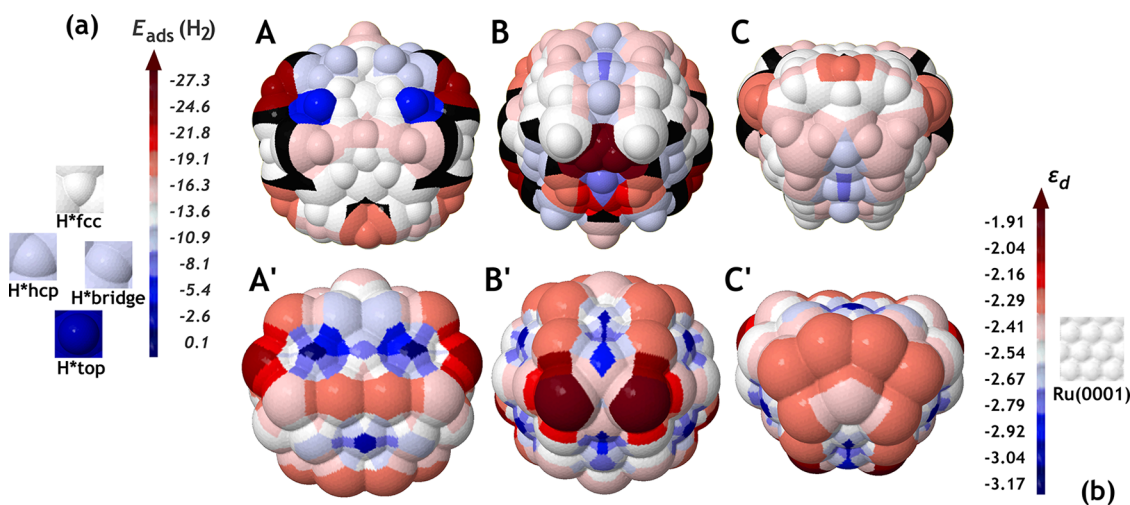

Figure 2. (a) Probing of the adsorption of H atoms at the surface of the Ru_{55}-MD NP. (A−C) different points of view of the map summarizing the dissociative adsorption energy of H_2. It is made by superposing 41 DFT calculations performed on $Ru_{55}H$ nanoclusters, that is, a total of 69 sites owing to the symmetry plane of the cluster. Each small CPK sphere is colored according to the energy scale (in kcal/mol) given on the right. Unprobed zones are shown in black. The corresponding mapping on the Ru(0001) surface is given in the insets (fcc, −13.6 kcal/mol, white; hcp and bridge, −11.9 and −10.1 kcal/mol, light blue; top; −3.3 kcal/mol, dark blue; values taken from ref 56). (b) $\bar{\varepsilon}_d(\mu_k)$ map of the Ru_{55}-MD cluster and ε_d energy scale. The orientations (A'−C') are given in the same order as in (A−C).

Ru(0001)-like facets with almost the same strength as calculated on Ru(0001) slabs (map **A**, Figure 2a); surface adsorption energies in the neighborhood of the subsurface defect are strong (−27.3 kcal/mol, map **B**); two other sites located at sharp ridges also have the propensity to strongly adsorb H atoms (−23.6 kcal/mol, map **A**); adsorption on edges is usually slightly larger than adsorption on flat surfaces (maps **A** and **C**). It is intriguing that adsorption of H atoms on two kinds of sites is found to be twice as strong as on fcc sites of Ru(0001). It is clearly a matter of selectivity of given sites at the surface of this nanocluster, which cannot be explained by $\langle \varepsilon_d \rangle$.

Analysis of the on-Site Adsorption Strength of Hydrides. We shall now evaluate whether the ε_d descriptor is able to account for these local adsorption strengths. For this purpose, eq 1 is now applied to each surface atom of a RuNP. In other words, this yields an effective d energy level for each surface atom, $\bar{\varepsilon}_d(\alpha)$, which is expected to linearly correlate with adsorption energies of ligands.

Yet, by definition μ-H and μ_3-H atoms are shared by two or three Ru atoms. The possible correlation between $\bar{\varepsilon}_d(\alpha)$ and adsorption energies of H atoms on triangular facets or bridges cannot be evaluated by a standard plot of $E_{ads}(H_2)$ versus $\bar{\varepsilon}_d(\alpha)$, which is an atomic descriptor related to atop adsorption only. A coordination counterpart of the atomic d-band center, $\bar{\varepsilon}_d(\mu_k)$, can however be calculated for each adsorption site by averaging the value of the Ru atoms possibly involved in such coordination. This is what is usually done to evaluate the d-band center value which characterizes special sites on surfaces, such as kinks or steps. Instead of plotting adsorption energies as a function of this coordination d-band center descriptor, we again propose a visual indication given as a color map (its construction is explained in the Methods section). This color map gives an immediate view of the possible spots for strong (dark red), normal (white) and weak (dark blue) adsorption with respect to Ru(0001), the origin of the ε_d energy scale being chosen as the value calculated for surface atoms of the [001] slab. The map obtained for Ru$_{55}$(MD) is given in Figure 2b, with the same points of view as the adsorption energies mapped in Figure 2a. There is a very satisfactory similarity between the $E_{ads}(H_2)$ and $\bar{\varepsilon}_d(\mu_k)$ maps. The same dark blue sites associated to very weak adsorption strengths are found in both representations; the dark red spots are found in the same areas of the surface; adsorption energies close to the −13.6 kcal/mol value found for the Ru(0001) surface are in line with $\bar{\varepsilon}_d(\mu_k)$ values close to the d-band center of the Ru(0001) plane, i.e., −2.54 eV. Some discrepancies can be observed for certain coordination sites: adsorption energies calculated for edge sites (map **C**, Figure 2a) are between ca. −19 and −13.6 kcal/mol, whereas the **C′** map suggests adsorption energies between −16 and −19 kcal/mol; the same comment applies to the ridge in the middle of

maps **A** and **A′**. These moderate inconsistencies indicate that the accuracy of the $\bar{\varepsilon}_d(\mu_k)$ index in predicting adsorption energies of H atoms on the surface is around ±3 kcal/mol for an energy range of 27 kcal/mol (i.e,. 10%). This value is low enough owing to the target of this work, i.e. finding an electronic descriptor that accounts for the adsorption energies calculated for the Ru$_{55}$(MD). It also confirms that the Ru(0001)-like part of this small cluster is similar to an infinite Ru(0001) slab, both in terms of adsorption energy and electronic fingerprint. Other sites with adsorption energies higher or lower than the −13.6 kcal/mol reference value are also well predicted by the $\bar{\varepsilon}_d(\mu_k)$ index, with the exception of the butterfly like pattern that lies above the subsurface vacancy. It is clear from the **B** and **B′** maps of Figure 2 that to some extent the $\bar{\varepsilon}_d(\mu_k)$ index fails in accurately estimating the localization of the site that favors the strongest adsorption on Ru$_{55}$(MD). According to the map it should happen on the two apexes of the butterfly like pattern lying above the subsurface vacancy (site **b**, Figure 3), whereas the strongest adsorption energy on atop sites is found on another Ru atom of the butterfly pattern (site **b′**). The local reorganization of the metal atoms of this pattern under H adsorption accounts for this difference. A careful similarity/structure analysis has shown that, upon adsorption, the atom moves away by ∼1.1 Å from its initial position - a somewhat large value. The mobility of this atom upon adsorption thus involves electronic reorganization and the transfer of the enhanced adsorption property in the neighborhood of the site identified by our descriptor. This gives a special site status to this butterfly like feature on the surface, both in terms of electronic structure and plasticity.

To conclude this part, the most promising success of the $\bar{\varepsilon}_d(\mu_k)$ index is its ability to quantitatively confirm that the highest adsorption energies calculated by this model cluster are related to the local availability of average d orbitals. Now that this descriptor has shown its potential to deal with hydrides adsorbed on a ≲1 nm cluster, its properties must be further assessed: does it account for the adsorption of other model ligands on the surface of Ru$_n$ nanoclusters?

Adsorption of X and L ligands on Ru$_n$ Nanoclusters (n = 55, 147). Three other ligands were considered in addition to H, namely the one-electron CH$_3$ ligand, the two-electron PH$_3$ ligand and CO ligands, the latter being a classical benchmark in surface- and nanoscience.[49] They were adsorbed on various atop, edge-bridging and face-capping coordination sites of low- and high-symmetry clusters, namely, Ru$_{55}$(MD), Ru$_{55}$(HCP) and Ru$_{55}$(IC), Ru$_{147}$(IC). These extensive DFT calculations of adsorption energies are plotted in Figure 3 versus $\bar{\varepsilon}_d(\mu_k)$, in addition to selected cases of hydrogen adsorption. The first comment is that whatever the coordination site, the ligands adsorb in the order CO > PH$_3$ > H > CH$_3$.
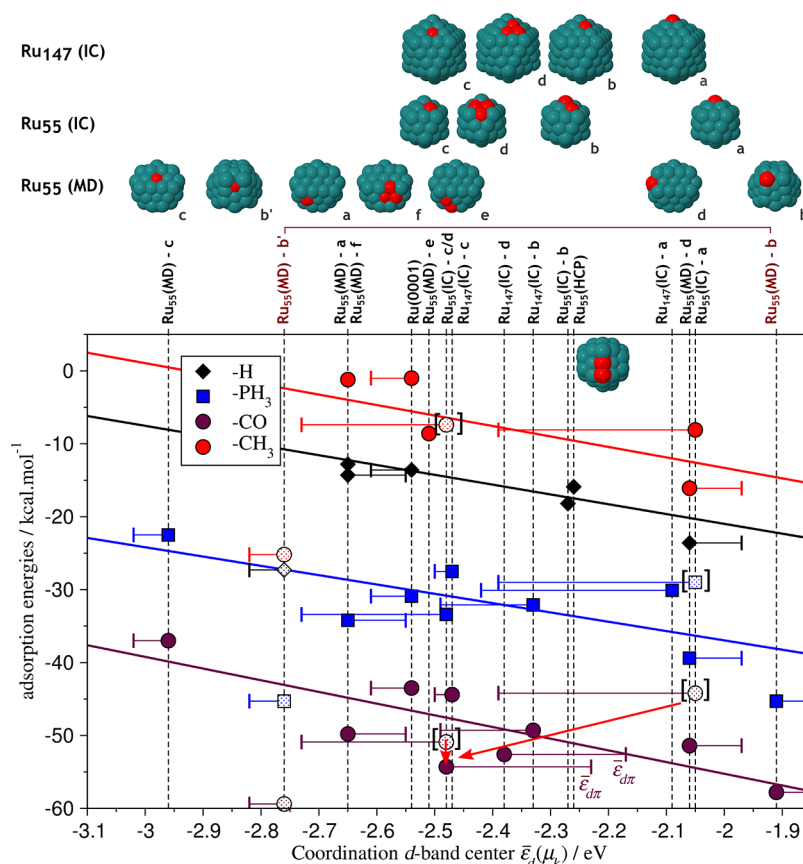
Figure 3. Adsorption energies (in kcal/mol) of H, CH_3, PH_3 and CO as a function of the d-band center calculated for various coordination sites of Ru_{55}(MD), Ru_{55}(IC), Ru_{55}(HCP), Ru_{147} (IC) and on the Ru(0001) slab. The coordination sites are indicated in red on the CPK models. CO and PH_3 are atop coordinated on Ru(0001), whereas CH_3 and H are adsorbed on the fcc site. In an attempt to understand the scattering, the d_{z^2}-projected d-band center value ($\varepsilon_{d\sigma}$) is indicated as an error bar for terminal ligands only (they can be straightforwardly identified by the CPK models which exhibit a single red marble). Another energy range based on the d_π-projected d-band center (the definition of $\varepsilon_{d\pi}$ is given in the Discussion section) is given for the d and b adsorption sites of and Ru_{147} (IC), respectively (see text for details). Second-order saddle points are also included on the figure, although they are not taken into account in the linear regression since these are metastable configurations (they are designated by square brackets, an arrow indicating which minima they connect for the CO case).

There is again a linear correlation between the adsorption energy of a ligand and $\bar{\varepsilon}_d(\mu_k)$. The main observation from Figure 3 is that the four slopes are very similar, with a significant dispersion. This confirms that there is an overall scaling behavior of adsorption energies that can be interpreted with the coordination d-band center. In other words, knowing both the adsorption energy of a ligand on a *unique* system (Ru(0001), for instance) and $\bar{\varepsilon}_d(\mu_k)$ should yield a good estimate of the adsorption energy of the ligand on *any* site of a RuNP, provided that its atomic-projected DOS has been calculated. But can the scatter of adsorption energies be explained, or must this ~6 kcal/mol deviation be considered as the intrinsic accuracy of such a simple monoelectronic descriptor? We are going to show that it does better than the apparent discrepancies observed in Figure 3. At first glance, the color map previously proposed is attractive because it is both simple and accurate in rationalizing the adsorption strength of H atoms on the surface of RuNPs. But coordination chemistry is more complicated than the simple interaction of the spherical 1s AO of an H atom with an effective d orbital. This is at the basis of the versatility of the interaction between metal atoms and main group ligands and it is related to the local symmetry of the orbitals involved: the d AOs of the metal and the σ and π active MOs of the ligands. This implies that the d-band center-based color map is a zeroth-order tool that must be improved by subtle arguments in line with molecular orbital theory and local symmetry.

This is what we intend to show from now on by analyzing in detail the results obtained for the CO functional group. First, the largest deviations are observed mainly for atop adsorption, *i.e.*, on the Ru_{55}(IC)-**a**, Ru_{55}(IC)-**c** and Ru_{55}(MD)-**a** sites. The adsorption energy of CO at an apex of Ru_{55}(IC) (**a** site) is significantly higher in energy than the values estimated from the $\bar{\varepsilon}_d(\mu_k)$ index, whereas it is the opposite for the **a** site in Ru_{55}(MD). But such discrepancies may not be surprising bearing in mind that, on the basis of ligand-field theory, an effective d level is unable to account for the

specific role of each d AO in the bonding. This means that it is necessary to take into account the ligand-field splitting created on a given atom by all other atoms. Following symmetry arguments, we propose to interpret the apparent discrepancy observed for some atop coordination in terms of the availability of the metal d orbital mainly involved in the atop bonding of σ-donor ligands, i.e., the d_{z^2} AO. The farther the distance to the Fermi level, the weaker the vertical adsorption energy. Its effective energy, $\varepsilon_{d\sigma}$, is systematically indicated as an error bar in Figure 3. Note that it is meaningful for atop adsorption sites only (these properties are gathered in Table S4). The error bar is narrow in some cases, i.e., there is only a slight deviation from the linear scale. It is large in other cases, and nicely explains that calculated adsorption energies are much lower than expected on the apexes of the icosahedral clusters. The trend given by an error bar usually reduces the scatter. But the adsorption of CO on an edge of the Ru_{55} icosahedron (site **c**) resists this simple rule of thumb. The $[\varepsilon - \varepsilon_{d\sigma}]$ energy range suggests that the adsorption energy of CO at site **c** should be lower than calculated. Actually, it turns out that the **a** and **c** $Ru_{55}(IC)CO$ structures are second-order saddle points which lead to μ-CO and finally to μ_3-CO (site $Ru_{55}(IC)$-**d** in Figure 3). The preference of CO for a μ_3 coordination site can be explained by analyzing in details the decomposition of the atomic d-projection of the DOS into its σ (d_{z^2}), π (d_{xz}, d_{yz}) and δ ($d_{x^2-y^2}$, d_{xy}) components, which, respectively, account for terminal and tilted adsorption of σ-donor ligands and for in-plane interaction (Scheme 1). The values reported in Table S4 show that, on average, the d_π effective AOs of edge atoms (structure $Ru_{55}(IC)$-**c**) are higher in energy than the d_σ effective AO (-2.2 eV vs -2.7 eV). The d_π effective AO orientated perpendicularly to the edge actually lies even higher (-1.9 eV). This suggests that a σ-coordinated ligand will rather be hooked by this AO and will consequently lie on the side of an edge. Owing to local symmetry, three edges will exert the same effect, resulting in the final μ_3 preference of CO for the center of the triangular facets and in a strong adsorption energy (-54.3 kcal/mol). This is in line with the $\varepsilon_{d\pi}$ index of the Ru edge atoms it is connected to. Taking into account the relationship between each orbital-driven adsorption site and the ε_d index each site is characterized by, significantly reduces the deviation with respect to the expected linear scaling. This is indicated by the coefficient of determination, R^2. In the CO case, whereas it is found to be 0.62 by considering $\bar{\varepsilon}_d$, it increases to 0.83 by taking into account the appropriate index (see also Figure S2).

Let us now briefly focus our attention on the L = PH_3 and L = CH_3 cases. The deviations with respect to the interpolation lines are usually similar to those observed for the ruthenium carbonyl NPs: the $Ru_{55}(IC)L$-**a** isomers lie significantly above the expected value; the
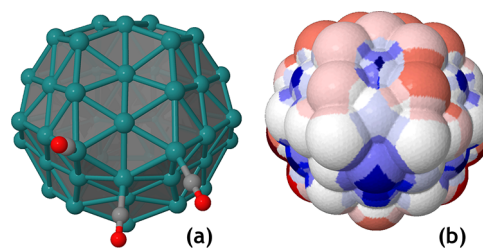

Figure 4. (a) Geometry of a $Ru_{55}(MD)(CO)_3$ cluster. The three carbon monoxide groups are simultaneously adsorbed on the butterfly like pattern. (b) d-band center map for the $Ru_{55}(MD)$ metallic core of $Ru_{55}(MD)(CO)_3$ (same orientation as B' in Figure 2b; for the sake of clarity, the CO groups are hidden).

$Ru_{55}(MD)PH_3$-**a** isomer is found to be slightly more stable than the $\bar{\varepsilon}_d$ estimation; the plasticity of the Ru_{55}-(MD)-**b**' site involves a strong stabilization upon adsorption of CH_3 and PH_3; as suggested by the $\varepsilon_{d\sigma}$ index, the adsorption of PH_3 on the $Ru_{55}(MD)$-**a** site is enhanced compared to $\bar{\varepsilon}_d$. In short, there is an overall consistency between ligands that have a σ-donor character and which also interact with the metal sites either through π-backbonding or by hyperconjugation.

It is also interesting to note that the saddle-point pattern found for some atop adsorption is obtained in the case of a large conflict between the d orbital availability of a site (given by $\bar{\varepsilon}_d(\alpha)$) and the atop unavailability revealed by a low $\varepsilon_{d\sigma}$ value, i.e., in case of a large $[\bar{\varepsilon}_d - \varepsilon_{d\sigma}]$ energy domain. No general rule can of course be drawn from such an observation, and a calculation of vibrational frequencies is the only appropriate way to identify saddle points. However, the computational cost of normal modes of vibration is prohibitive for the largest compounds. A guiding rule of thumb may also be useful as a part of a d-band center-based prescreening process of possible active sites. All the cases investigated in this paper indicate that a strong contradiction between an energy-accessible ε_d level and a deep $\varepsilon_{d\sigma}$ level may result in a lower atop adsorption strength than expected according to ε_d or may reveal the transition state nature of the site.

Influence of the Ligands on the Electronic Fingerprint of Surface Atoms. The influence of preadsorbed surface ligands on the adsorption strength of co-adsorbed species is also a key point. It deserves a dedicated study and we shall here only address the question of the modification of the coordination d-band center, $\bar{\varepsilon}_d(\mu_k)$, upon adsorption of CO ligands on the $Ru_{55}(MD)$ model. In this preliminary study, we only considered the simultaneous adsorption of 3 CO ligands on the butterly like site which lies above the subsurface vacancy (Figure 4a). The average adsorption energy per CO group is -48.4 kcal/mol, i.e., still slightly larger than on the Ru(0001) surface (-43.5 kcal/mol) but significantly lower than the adsorption of a single CO on the optimal **b**' site (-59.3 kcal/mol).
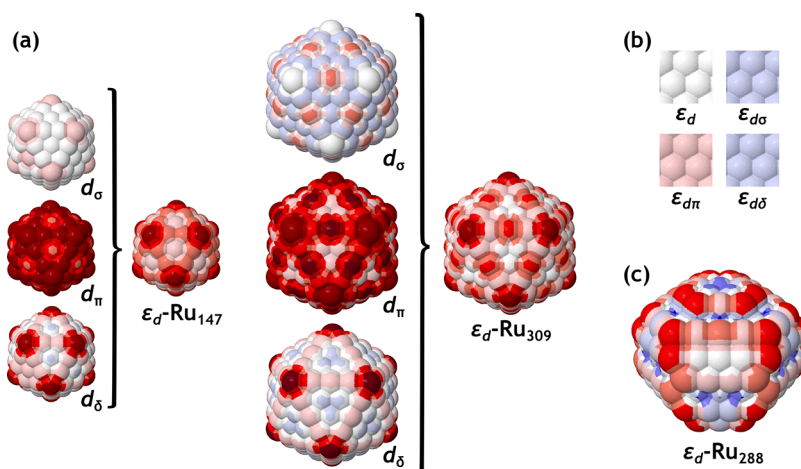
Figure 5. (a) d-band center coordination maps for Ru_{147} and Ru_{309} icosahedral NPs. The d_π-, d_δ- and d_σ-projected maps are shown as well; (b) $\varepsilon_{d\sigma}$ (−2.61 eV), $\varepsilon_{d\pi}$ (−2.38 eV) and $\varepsilon_{d\delta}$ (−2.68 eV) maps calculated for the surface atoms of the Ru(0001) slab (see also Table S4). (c) d-band center map for an ∼1.8 nm Ru_{288} hcp NP. A Wulff construction gave the basic particle spherical shape. An edge row of atoms was removed between the (001) and (101) planes, giving rise to steps that exhibit B_5 sites. We followed the assumption formulated in ref 4, later confirmed by DFT calculations,[5] which showed that the (001)/(101) edges lower their energy by a reconstruction in which the edge row of atoms is removed. According to ε_d, the most active sites for adsorption are the upper steps of the B_5 sites and the edges between the {110} facets.

The deformation of the site which maximizes the adsorption strength for a single CO cannot simultaneously favor the co-adsorption of three CO groups to the same extent. It is interesting to note that the adsorption energy expected by plotting the ε_d parameter averaged for these three atoms (−2.25 eV) on the linear interpolation given in Figure 3 nicely fits the calculated value (−50 kcal/mol *vs* −48.4 kcal/mol). The d-band center map calculated for the Ru_{55} metallic core of $Ru_{55}(CO)_3$ plot on Figure 4b can be compared with the **B′** map of Figure 2. With the exception of the three metal sites on which the CO groups are coordinated, the maps look very similar. We postulate from this single case that even in a small nanocluster, the species adsorbed only have a short-range impact on the electronic properties of the NPRu core and therefore on the adsorption energies of other species on the other sites.

DISCUSSION AND REFINEMENT OF THE MODEL

On the Necessity To Improve the d-Band Center. The $\bar{\varepsilon}_d(\mu_k)$ descriptor is a good index for explaining and estimating adsorption energies on all coordination sites available on the surface of ruthenium NPs. It was shown by the extensive study of H adsorption on several sites of a $Ru_{55}(MD)$ model cluster and further confirmed by considering other X (CH_3) and L (PH_3 and CO) ligands on Ru_{55} and Ru_{147} clusters. The associated trustworthiness range of this index is *ca.* 5 kcal/mol. The strongest deviations were observed for saddle points, and on local plasticity of the surface. The so-called butterfly site turns out to be a prototype of the possible enhancement of the adsorption strength of a ligand upon surface deformation, in relation with the existence of a subsurface vacancy. In addition to this

remarkable special site, the largest discrepancies, observed for atop adsorption, were mainly explained for CO by analyzing in detail the electronic structure of the metal surface and its compatibility with the electronic features of the ligands adsorbed. CO adsorption is ruled out by the interaction of its highly directional σ HOMO and of its π^* MOs with the metal surface. But whereas the metal-to-ligand π interaction is expected to be important for hollow site adsorption, it is weak for atop site adsorption.[57] This suggests that the $\bar{\varepsilon}_d(\mu_k)$ index, averaged over the five d components, may provide only a rough indication of the possible atop adsorption strength since the metal atomic orbital most involved in the bonding with CO is the d_{z^2} AO. Our analysis has shown that the $\bar{\varepsilon}_d(\mu_k)$ descriptor, although reasonably accurate, only provides a zeroth order estimation of *local* adsorption energies. It has been improved by doing a projection along each σ, π and δ component. This yields an indication of the propensity of a metal site to hook a ligand owing to the symmetry of the ligands' MOs primarily involved in bonding.

d AOs-Projected Maps. This is why we now propose to complete the d-band center map proposed in this study by d_σ, d_π and d_δ maps, such as those plot in Figure 5a for Ru_{147}(IC) and Ru_{309}(IC). The high symmetry of these icosahedral RuNPs sheds light on the relationship between local electronic fingerprint, adsorption properties and quantum-size effect (more usual energy-level diagrams are given in Figure S5). As already explained, such decomposition allows refinement of the conclusions arising from $\bar{\varepsilon}_d(\mu_k)$ and avoids spurious analysis. This is the case for the atop adsorption of ligands on the apexes and edges of these species. According to this descriptor it is expected to

be stronger than the adsorption on Ru(0001), but the maps clearly show that the apparent availability of the effective d level results from the high energy-lying d_π and d_δ effective AOs. The d_σ map is actually close to being white everywhere. This suggests an adsorption energy on apexes close to adsorption on Ru(0001). In contrast, the dark red zones in the d_π and d_δ maps indicate that ligands with a highly directional σ orbital should attack these sites sideways. According to local symmetry, the resulting adsorption could even be enhanced by a favorable π interaction. It was observed for Ru$_{55}$(IC), CO adsorbing strongly at the center of triangular facets, in relation with a high ε_{d_π} index value (see Figure 3). Another important conclusion arising from these calculations of adsorption properties at the surface of the icosahedral RuNPs is that "edges" and "apexes" do not systematically mean "strong adsorption". It depends on the local electronic structure involved both by the local topology of the surface and by other atoms.

Quantum-Size Effect in RuNPs. This can be discussed by comparing the maps plotted for Ru$_{147}$(IC), Ru$_{309}$(IC) and Ru(0001) (Figure 5a,b). First, the apexes and edges of the two icosahedrons also have similar electronic fingerprints, with the exception of the atom that lies at the middle of the edge in Ru$_{309}$. More interestingly, the atoms belonging to the triangular facets in this NP exhibit the same d, d_σ, d_π and d_δ electronic features as the surface atoms of the Ru(0001) slab. As suggested by these indexes, although the triangular facets in Ru$_{147}$(IC) are far from being extended planes, adsorption of ligands on the central atom is expected to be only slightly stronger. Again, this means that it is the local topology of surfaces that rules the adsorption properties in large RuNPs; NPs that would mainly offer facets reminiscent of the Ru(0001) plane and a small number of special active sites should not exhibit an optimized catalytic activity with respect to Ru(0001) heterogeneous catalysts.

Electronic Fingerprint of the Highly Active B$_5$ Sites. The icosahedral structures are interesting because of their high symmetry which reveals global trends more clearly than clusters with an irregular surface. But it has been shown both experimentally[58] and theoretically[5] that colloidal RuNPs are spherical crystals that adopt the hcp structure of bulk ruthenium. Owing to this, our study would not be complete without an analysis of the electronic property of an hcp RuNP with realistic size. An important result in the context of adsorption properties on RuNPs is the presence of steps, the so-called B$_5$ sites,[4] that have been proven to be active with respect to the dissociation of the nitrogen molecule.[5] Since hardly any B$_5$ sites will occur on small RuNPs, we considered a large spherical NP made of 288 atoms. Its $\bar{\varepsilon}_d(\mu_k)$ map is plotted in Figure 5c and the AO-projected indices are given in Table S4. It is remarkable that the upper steps of these special sites are characterized by a

high ε_d value (-2.26 eV), although they are not as active as the **b** and **b**′ special sites in Ru$_{55}$(DM) (-1.91 eV for **b**). But what is notable in the present case is that d_σ, d_π and d_δ effective AOs are close in energy. This highlights the correspondence between a narrow bandwidth on such sites with a small degeneracy lift of the five effective d AOs. They are *all* energetically available for subsequent reaction and this may give a versatile active property to these B$_5$ sites. Let us address again the matter of quantum size effects. The upper step of the B$_5$ sites has the same effective energy levels both in Ru$_{288}$ and in the Ru-(10$\bar{1}$5) model crystallographic plane. Lastly, unlike the edges on the icosahedral NPs, those that also appear in red in Figure 5c (and in gray in Table S4) are also characterized by almost degenerate d effective AOs. We can thus assume that these sites could also have a remarkable activity in catalytic processes involving RuNPs.

Practical Interest of the Scaling Properties of Adsorption Energies. The model has the power to predict adsorption energies of any ligand by the knowledge of its adsorption energy at a unique site. To illustrate this comment, let us consider the adsorption of the methyl tin group SnMe at the fcc site of the Ru(0001) surface. It is strongly bound by -81 kcal/mol, the largest value calculated in this work. As a consequence, such ligand, which could stem from the decomposition of HSnMe$_3$, can efficiently poison the surface of Ru nanocatalysts. The scaling behavior observed in Figure 3 implies that its adsorption in the close neighborhood of the **b** and **b**′ site in Ru$_{55}$(MD) should be enhanced roughly by $10-15$ kcal/mol (the slope is the same for all ligands, whereas the adsorption energy of SnMe on Ru(0001) yields the y-intercept). This is confirmed by DFT calculations (-94.0 kcal/mol). This further result confirms that the $\bar{\varepsilon}_d$ index provides good estimations for adsorption energies.

CONCLUSION AND OUTLOOK

A new model accounting for the adsorption strength of ligands on the surface of Ru NPs has been developed in this paper. It is based on the d-band center model of Hammer and Nørskov,[32] whose seminal formulation turns out to be a global property of metal surfaces or special sites, poorly able to accurately account for selective processes at the surface of transition metal NPs. Our model in contrast is defined as an on-site energy-weighted projection of the density of states on individual d AOs. The resulting $\bar{\varepsilon}_d$ and ε_{d_m} indexes for adsorption energy are conveniently depicted as color maps directly accounting for thermodynamics at the surface of the RuNPs. The most interesting sites according to the original averaged atomic d-band center $\bar{\varepsilon}_d$ can then be more deeply analyzed in terms of the d AOs decomposition of this index and followed up by full DFT calculations. Such decomposition has a

broader meaning and this is where the atomic d-band center proposed in this paper closely meets standard molecular orbital chemistry: it provides effective d AO energy levels for each surface atom in its environment. In other words, it is the result of the ligand field generated by the other surface and core metal atoms, as well as by other surface species. It is a very interesting result since, to some extent, we can take advantage of the powerful rationalization offered by ligand-field theory for molecular systems in order to understand the chemistry of surface atoms in transition metal NPs. If M is a surface metal atom, its further adsorption ability is characterized by the energy splitting of its effective d AOs (Scheme 1); the adsorption of a ligand L on this metal atom can then be understood in terms of a fragment orbital analysis of the reaction M + L → M−L, and it may not be inappropriate to assume that a good knowledge of orbital interactions in chemistry[50] could partially be transposed to understanding the local surface properties of metal NPs. According to our model, a RuNP must not be seen as a piece of metal with a delocalized electronic structure that rules adsorption on its surface: to some extent, it must be viewed as an assembly of mono- (atop), di- (edge-bridging), tri- (face-capping) or event tetra- (μ_4) nuclear complexes with effective electronic fingerprints resulting from interactions with other atoms. In other words, the adsorption strength on a site is directly related to the ligand field exerted by the other atoms and depends on the topology of this site. The local symmetry involves a specific energy splitting of the d AOs, whereas the environment may modulate the amplitude of the splitting and the position of the average energy, $\bar{\varepsilon}_d(\alpha)$. On the basis of these DFT calculations, we have shown that, for Ru NPs, the ligand field is already as strong in small clusters as in model surfaces (see for example the planar facet of Ru$_{55}$(MD) vs Ru(0001) and the B$_5$ sites in Ru$_{288}$ and in the Ru(10$\bar{1}$5) slab). This is one of the important outcomes of the present work.

Following all these assumptions and conclusions, we shall now propose to revisit the Sabatier principle. According to the qualitative concept of Paul Sabatier, catalytic properties will be hindered if the reactants adsorb too strongly, whereas no reaction will occur if the interaction is too weak. The Sabatier principle applied to the NP case is illustrated by the monoelectronic descriptors introduced in this paper and given as color maps: hot spots for adsorption are shown in red, blue identifies potentially weak interactions, whereas white shows where intermediate adsorption processes should occur. The arbitrariness of the color scale is obvious, but the white which is defined by the electronic feature of the Ru(0001) facet. In addition, the B$_5$ sites appear in red, in agreement with a stronger adsorption strength of ligands on such special sites and with a well-known high activity.[5] It may thus be

assumed that the red color on these maps identifies ideal sites at the surface of Ru NPs. It may be the case, and $\bar{\varepsilon}_d$ can already be an appropriate descriptor for evaluating the catalytic performance of a site. But we postulate that the critical concept is that interactions between catalysts and reactants will be facilitated by the availability of the local electronic structure of the nanocatalyst. This property is quantitatively given by the $\varepsilon_{d\sigma}, \varepsilon_{d\pi}$ and $\varepsilon_{d\delta}$ descriptors, which allow to refine the conclusions based on the original on site d-band center, $\bar{\varepsilon}_d$: a powerful catalytic site may be identified both by an appropriate $\bar{\varepsilon}_d$ value and by an appropriate ligand-field splitting. This was highlighted for the B$_5$ sites, which are characterized both by a small degeneracy lift and a similar energetic availability of the five effective d AOs of the upper step atom. Given the relationship between the shape and effective energy of these AOs (Scheme 1) and their overlap with the active MOs of an adsorbate (i.e., relevant to the catalytic process), we conjecture that a catalytic activity will be maximized by optimizing the energy of the effective d AOs of the active sites. This can be achieved by modulating the ligand-field exerted on the surface metal atoms.

Another interesting conclusion of this work is the scaling properties of the adsorption energies, systematically shown whatever the ligand (H, CO, PH$_3$ and CH$_3$). To the best of our knowledge, whereas they are now generally accepted for transition-metal surfaces,[59] this is the first time that they have been found for individual adsorption sites at the surface of nanoparticles. The predictive character of this property has been checked for a tin ligand on one of the special sites considered in this paper. Incidentally, an enhanced adsorption property due to the presence of a subsurface vacancy has been found.

Although our model is currently developed in the context of the PBE functional and PAW based periodic calculations, it is expected to exhibit the same consistency between adsorption energies and d-band center maps whatever the method for calculating the energy. It will be applied to other metals in order to quantify the variation in catalytic activities from one metal to another. However, several conclusions arising from this work are probably transferable to other medium-to-late transition metal NPs. A similar analysis for noble metal and magnetic NPs is in progress, the model being completed by taking into account the role of the s density of states and d-band filling. In the present paper, the BEP relation between the activation energy and the reaction energy is assumed implicitly to hold for reactions that occur at the surface of RuNPs. The confirmation that activation energies of model reactions follow reaction energies and the trends given by the descriptors proposed in this paper is also currently investigated. The model is expected to contribute

to bridging the gap between molecular inorganic chemistry and nanochemistry and it opens the route to the rational design of efficient transition metal nanocatalysts.

METHODS

DFT Calculations. All computations were performed within the framework of the density functional theory (DFT) considering the spin unpolarized or polarized constraint, depending on the system under study. The exchange-correlation potential was approximated by the generalized gradient approach proposed by Perdew, Burke, and Ernzerhof (PBE).[60] Calculation of energy parameters as well as geometry optimization were carried out using projector augmented waves (PAW) full-potential reconstruction[61,62] implemented in the Vienna *ab initio* simulation package, VASP.[63,64] To minimize errors arising from the frozen core approximation, we used the PAW data sets treating the 4p, 4d and 5s Ru states (14 valence electrons). As already proposed in a previous paper,[56] we found that a kinetic energy cutoff of 280 eV was sufficient to achieve a total energy convergence within several millielectronvolts for H adsorption. A cutoff of 500 eV was used in the case of phosphine, methyl, tin and carbonyl compounds. For the geometry optimizations of clusters, a Γ-centered[65] calculation was used, with a Gaussian smearing of 0.02 eV width for the partial occupancies. Atoms were free to move until the residual forces on any direction were less than 0.02 eV/Å. The supercell size is set to ensure a vacuum space of *ca.* 16 Å between periodic images of Ru_n clusters ($25 \times 25 \times 26$ Å for Ru_{55}, $30 \times 30 \times 31$ Å for Ru_{147} and $45 \times 45 \times 46$ Å for Ru_{309}). These parameters were tested and proven to be sufficient to accurately model the ruthenium clusters dressed by ligands for a reasonable computational cost. The DOS was determined by setting up the same parameters. The surfaces

were modeled by a periodic six-layer metal slab, and the ligands were adsorbed on one side of the slab. The computational details are the same as those used in ref 56. Atomic and averaged d-band centers were calculated with our home-made tools4vasp suite of utilities. We used some test cases to check that we found the same $\langle \varepsilon_d \rangle$ values as the program developed by Henkelman's group.[66] The harmonic vibrational modes were calculated for certain clusters in order to distinguish minima and saddle points by using the dynamical matrix code implemented in VASP as well as the VASPTST tools also developed by Henkelman's group. Adsorption energies were calculated according to the formula $E_{ads}(L) = (1/m)[E(Ru_nL_m) - E(Ru_n) - (m/k)E(L)]$, where L = H_2 ($k = 2$), CO ($k = 1$), $(CH_3)_2$ ($k = 2$), PH_3 ($k = 1$). In the case of H_2 and C_2H_6, E_{ads} is a dissociative adsorption energy: it provides the stabilization energy of H atoms or methyl groups, and includes the cost of a H−H or C−C bond breaking.

Construction of a d-Band Center Based Coordination Map. As explained earlier, we assessed the adsorption strength around each surface atom of ruthenium NPs by means of $\bar{\varepsilon}_d(\alpha)$, the energy-weighted DOS projected on all d atomic orbitals of a surface atom α. This atomic d-band center can be nicely depicted as a color map, which provides a first overview of the d-accessibility of an atomic site (see Figure 6, top representation). ε_d is not expected to be accurate enough to account for slight differences in adsorption strength between two neighboring coordination sites. But the on-top representation does not explicitly show that simultaneous adsorption on two weakly bonding (blue) and strongly bonding (red) sites is expected to be moderate (white). As explained earlier, a coordination d-band center $\bar{\varepsilon}_d(\mu_k)$ color map was chosen as a better visual indicator of adsorption strength. $\bar{\varepsilon}_d$ for a coordination site μ_k is simply calculated as an average of the $\bar{\varepsilon}_d(\alpha)$ values of all surface metal atoms involved in such bonding (eq 1).

The final map is obtained as a superposition of the $\bar{\varepsilon}_d$ values calculated for atop, edge-bridging, face- and square-capping sites (map in the upper part of Figure 6). The d_σ, d_π and d_δ indices proposed in this work were obtained respectively by projecting the DOS on the d_{z^2} AO only, on the d_{xz} and d_{yz} AOs, and on the $d_{x^2-y^2}$ and d_{xy} AOs:

$$\varepsilon_{d_m}(\alpha) = \frac{\left(\displaystyle\int_{E_{min}}^{E_F} \varepsilon n_{d_m}(\alpha, \varepsilon) \, d\varepsilon \right)}{\left(\displaystyle\int_{E_{min}}^{E_F} n_{d_m}(\alpha, \varepsilon) \, d\varepsilon \right)} \tag{3}$$

where $m = z^2, xz, yz, x^2 - y^2, xy$. Mind that the choice of coordinates is important since it is not unique. The z axis was systematically set up as being orthogonal to the local average surface the considered adsorption site belongs to, *i.e.*, it is oriented along the on-top coordination site in the case of terminal coordination. The two d_π and d_δ components may differ in some cases owing to local symmetry. For example, the in-plane y axis was set up as collinear to edges, as shown in Scheme 1. It involves that the d_σ, d_π and d_δ effective energies plotted as maps in Figure 5 or given in the Supporting Information (Table S4 and Figure S5) be required to perform several DOS projections by setting up an appropriate orientation of the NPs as a function of each considered coordination site.

ε_d

-1.91
-2.04
-2.16
-2.29
-2.41
-2.54
-2.67
-2.79
-2.92
-3.04
-3.17

Ru(0001)

=

top

+

edge-bridging
$\varepsilon_d(\mu)$

+

face-capping
$\varepsilon_d(\mu_3)$

+

square-capping
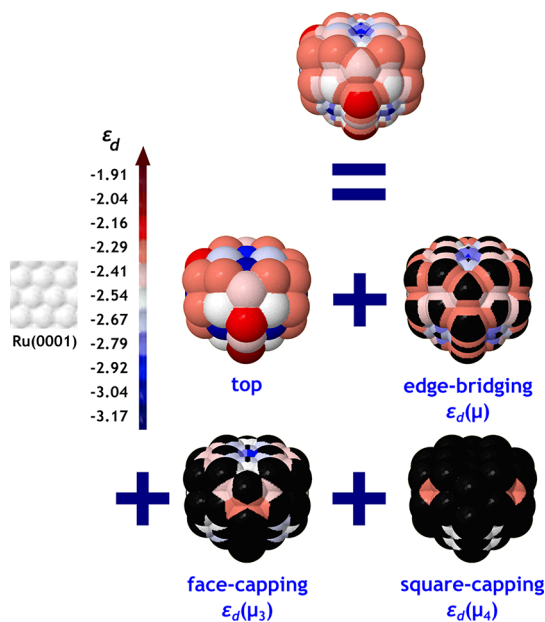$\varepsilon_d(\mu_4)$

Figure 6. Construction of the d-band center-based coordination map as a superposition of the d-band center (ε_d, in eV) projected on all surface top, μ, μ_3 and μ_4 coordination sites of the Ru_{55}-hcp nanocluster. The correspondence between colors and energy scale (in eV) is given on the left: the darker the red, the closer to the Fermi level; the darker the blue, the more stable the d-band center. The surface Ru(0001) average d-band center value (−2.54 eV) was chosen as the origin of this scale, whereas the top of the scale is set up to the highest ε_d found in the calculated clusters and NPs, *i.e.*, in the Ru_{55}(MD) nanocluster.

Conflict of Interest: The authors declare no competing financial interest.

REFERENCES AND NOTES

1. Halperin, W. P. Quantum Size Effects in Metal Particles. *Rev. Mod. Phys.* **1986**, *58*, 533–606.

2. Taylor, H. S. A Theory of the Catalytic Surface. *Proc. R. Soc. London, Ser. A* **1925**, *108*, 105–111.

3. Hammer, B. Special Sites at Noble and Late Transition Metal Catalysts. *Top. Catal.* **2006**, *37*, 3–16.

4. van Hardeveld, R.; van Montfoort, A. The Influence of Crystallite Size on the Adsorption of Molecular Nitrogen on Nickel, Palladium and Platinum: an Infrared and Electron-microscopic Study. *Surf. Sci.* **1966**, *4*, 396–430.

5. Honkala, K.; Hellman, A.; Remediakis, I. N.; Logadottir, A.; Carlsson, A.; Dahl, S.; Christensen, C. H.; Nørskov, J. K. Ammonia Synthesis from First-principles Calculations. *Science* **2005**, *307*, 555–558.

6. Bond, G. C.; Coq, B.; Dutartre, R.; Ruiz, J. G.; Hooper, A. D.; Proietti, M. G.; Sierra, M. C. S.; Slaa, J. C. Effect of Various Pretreatments on the Structure and Properties of Ruthenium Catalysts. *J. Catal.* **1996**, *161*, 480–494.

7. Six, C.; Beck, K.; Wegner, A.; Leitner, W. Ligand Effects in Novel Ruthenium-Based ROMP Catalysts Bearing Bidentate Phosphines. *Organometallics* **2000**, *19*, 4639–4642.

8. Roucoux, A. In *Topics in Organometallic Chemistry: Surface and Interfacial Organometallic Chemistry and Catalysis*; Copéret, C., Chaudret, B., Ed.; Springer-Verlag: Heidelberg, 2005; Vol. 16; Chapter Stabilized Noble Metal Nanoparticles: An Unavoidable Family of Catalysts for Arene Derivative Hydrogenation, pp 261–279.

9. Jansat, S.; Picurelli, D.; Pelzer, K.; Philippot, K.; Gómez, M.; Muller, G.; Lecante, P.; Chaudret, B. Synthesis, Characterization and Catalytic Reactivity of Ruthenium Nanoparticles Stabilized by Chiral N-Donor Ligands. *New J. Chem.* **2006**, *30*, 115–122.

10. Maitlis, P. M. Fischer–Tropsch, Organometallics, and Other Friends. *J. Organomet. Chem.* **2004**, *689*, 4366–4374.

11. McQuire, M. W. Rochester, C. H. FTIR Study of CO/H$_2$ Reactions over Ru/TiO$_2$ and Ru-Rh/TiO$_2$ Catalysts at High Temperature and Pressure. *J. Catal.* **1995**, *157*, 396–402.

12. Gerber, I. C.; Poteau, R. In *Nanomaterials in Catalysis*; Serp, P., Philippot, K., Eds.; Wiley-VCH: Weinheim, 2013; Chapter Theoretical Nanocatalysis: Where Are We Now?

13. Niu, S.; Hall, M. B. Theoretical Studies on Reactions of Transition-Metal Complexes. *Chem. Rev.* **2000**, *100*, 353–406.

14. Sautet, P.; Delbecq, F. Catalysis and Surface Organometallic Chemistry: A View from Theory and Simulations. *Chem. Rev.* **2010**, *110*, 1788–1806.

15. Nørskov, J. K.; Abild-Pedersen, F.; Studt, F.; Bligaard, T. Density Functional Theory in Surface Chemistry and Catalysis. *Proc. Natl. Acad. Sci. U.S.A.* **2011**, *108*, 937–943.

16. Shang, C.; Liu, Z.-P. Origin and Activity of Gold Nanoparticles as Aerobic Oxidation Catalysts in Aqueous Solution. *J. Am. Chem. Soc.* **2011**, *133*, 9938–9947.

17. Chin, Y.-H. C.; Buda, C.; Neurock, M.; Iglesia, E. Selectivity of Chemisorbed Oxygen In C-H Bond Activation and CO Oxidation and Kinetic Consequences for CH$_4$-O$_2$ Catalysis on Pt and Rh Clusters. *J. Catal.* **2011**, *283*, 10–24.

18. Liotard, D.; Penot, J.-P. In *Numerical Methods in the Study of Critical Phenomena*; Della Dora, J., Demongeot, J., Lacolle, B., Eds.; Springer: Berlin, Heidelberg, New York, 1981; p 213; Proceedings of a colloquium, Carry-le-Rouet, France, June 2–4, 1980.

19. Jónsson, H.; Mills, G.; Jacobsen, K. W. In *Classical and Quantum Dynamics in Condensed Phase Simulations*; Berne, B. J., Ciccotti, G., Coker, D. F., Eds.; World Scientific Publishing Co.: Singapore, 1998; Chapter Nudged Elastic Band Method for Finding Minimum Energy Paths of Transitions, pp 385–404.

20. Sheppard, D.; Terrell, R.; Henkelman, G. Optimization Methods for Finding Minimum Energy Paths. *J. Chem. Phys.* **2008**, *128*, 134106-1–10.

21. Remediakis, I.; Lopez, N.; Nørskov, J. CO Oxidation on Gold Nanoparticles: Theoretical Studies. *Appl. Catal., A* **2005**, *291*, 13–20.

22. Lanzani, G.; Nasibulin, A. G.; Laasonen, K.; Kauppinen, E. I. CO Dissociation and CO plus O Reactions on a Nanosized Iron Cluster. *Nano Res.* **2009**, *2*, 660–670.

23. Jiang, T.; Mowbray, D. J.; Dobrin, S.; Falsig, H.; Hølbaek, B.; Bligaard, T.; Nørskov, J. K. Trends in CO Oxidation Rates for Metal Nanoparticles and Close-Packed, Stepped, and Kinked Surfaces. *J. Phys. Chem. C* **2009**, *113*, 10548–10553.

24. Viñes, F.; Lykhach, Y.; Staudt, T.; Lorenz, M. P. A.; Papp, C.; Steinrueck, H.-P.; Libuda, J.; Neyman, K. M.; Görling, A. Methane Activation by Platinum: Critical Role of Edge and Corner Sites of Metal Nanoparticles. *Chem.—Eur. J.* **2010**, *16*, 6530–6539.

25. Lanzani, G.; Laasonen, K. NH$_3$ Adsorption and Dissociation on a Nanosized Iron Cluster. *Int. J. Hydrogen Energy* **2010**, *35*, 6571–6577.

26. Pei, Y.; Shao, N.; Gao, Y.; Zeng, X. C. Investigating Active Site of Gold Nanoparticle Au$_{55}$(PPH$_3$)$_{12}$Cl$_6$ in Selective Oxidation. *ACS Nano* **2010**, *4*, 2009–2020.

27. Roldan, A.; Manel Ricart, J.; Illas, F.; Pacchioni, G. O$_2$ Adsorption and Dissociation on Neutral, Positively and Negatively Charged Au$_n$ (n = 5–79) clusters. *Phys. Chem. Chem. Phys.* **2010**, *12*, 10723–10729.

28. Filot, I. A. W.; Shetty, S. G.; Hensen, E. J. M.; van Santen, R. A. Size and Topological Effects of Rhodium Surfaces, Clusters and Nanoparticles on the Dissociation of CO. *J. Phys. Chem. C* **2011**, *115*, 14204–14212.

29. Kim, H. Y.; Lee, H. M.; Henkelman, G. CO Oxidation Mechanism on CeO$_2$-Supported Au Nanoparticles. *J. Am. Chem. Soc.* **2012**, *134*, 1560–1570.

30. Fajin, J. L. C.; Bruix, A.; Cordeiro, M. N. D. S.; Gomes, J. R. B.; Illas, F. Density Functional Theory Model Study of Size and Structure Effects on Water Dissociation by Platinum Nanoparticles. *J. Chem. Phys.* **2012**, *137*, 034701.

31. Peterson, A. A.; Grabow, L. C.; Brennan, T. P.; Shong, B.; Ooi, C.; Wu, D. M.; Li, C. W.; Kushwaha, A.; Medford, A. J.; Mbuga, F.; *et al.* Finite-Size Effects in O and CO Adsorption for the Late Transition Metals. *Top. Catal* **2012**, *55*, 1276–1282.

32. Hammer, B.; Nørskov, J. K. Electronic Factors Determining the Reactivity of Metal Surfaces. *Surf. Sci.* **1995**, *343*, 211–220.

33. Hammer, B.; Nørskov, J. In *Impact of Surface Science on Catalysis*; Gates, B. C., Knozinger, H., Eds.; Advances in Catalysis; Academic Press: San Diego, CA, 2000; Vol. 45, pp 71–129.

34. Brönsted, J. N. Acid and Basic Catalysis. *Chem. Rev.* **1928**, *5*, 231–338.

35. Evans, M. G.; Polanyi, M. Inertia and Driving Force of Chemical Reactions. *Trans. Faraday Soc.* **1938**, *34*, 11–24.

36. Sabatier, P. Hydrogénations et Déshydrogénations par Catalyse. *Ber. Dtsch. Chem. Ges.* **1911**, *44*, 1984–2001.

37. Toulhoat, H.; Raybaud, P. Kinetic Interpretation of Catalytic Activity Patterns Based on Theoretical Chemical Descriptors. *J. Catal.* **2003**, *216*, 63–72.

38. Swiegers, G. *Mechanical Catalysis: Methods of Enzymatic, Homogeneous, and Heterogeneous Catalysis*; John Wiley and Sons, Inc.: New-York, 2008.

39. Tedsree, K.; Chan, C. W. A.; Jones, S.; Cuan, Q.; Li, W.-K.; Gong, X.-Q.; Tsang, S. C. E. ^{13}C NMR Guides Rational Design of Nanocatalysts *via* Chemisorption Evaluation in Liquid Phase. *Science* **2011**, *332*, 224–228.

40. Balandin, A. In *Modern State of the Multiplet Theory of Heterogeneous Catalysis*; Eley, D. D., Pines, H., Weisz, P. B., Eds.; Advances in Catalysis; Academic Press: New York, 1969; Vol. 19, pp 1–210.

41. Bligaard, T.; Nørskov, J.; Dahl, S.; Matthiesen, J.; Christensen, C.; Sehested, J. The Brønsted-Evans-Polanyi Relation and the Volcano Curve in Heterogeneous Catalysis. *J. Catal.* **2004**, *224*, 206–217.

42. Nørskov, J. K.; Bligaard, T.; Rossmeisl, J.; Christensen, C. H. Towards the Computational Design of Solid Catalysts. *Nat. Chem.* **2009**, *1*, 37–46.

43. van Santen, R. A.; Neurock, M.; Shetty, S. G. Reactivity Theory of Transition-Metal Surfaces: A Brønsted-Evans-Polanyi Linear Activation Energy-Free-Energy Analysis. *Chem. Rev.* **2010**, *110*, 2005–2048.

44. Jacobsen, C.; Dahl, S.; Clausen, B.; Bahn, S.; Logadottir, A.; Nørskov, J. Catalyst Design by Interpolation in The Periodic Table: Bimetallic Ammonia Synthesis Catalysts. *J. Am. Chem. Soc.* **2001**, *123*, 8404–8405.

45. Nørskov, J. K.; Scheffler, M.; Toulhoat, H. Density Functional Theory in Surface Science and Heterogeneous Catalysis. *MRS Bull.* **2006**, *31*, 669–674.

46. Anh, N. T. *Frontier Orbitals: A Practical Manual*; Wiley-VCH: Weinheim, Germany, 2007.

47. Hammer, B.; Morikawa, Y.; Nørskov, J. K. CO Chemisorption at Metal Surfaces and Overlayers. *Phys. Rev. Lett.* **1996**, *76*, 2141–2144.

48. Hoffmann, R. *Solids And Surfaces. A Chemist's View of Bonding in Extended Structures*; Wiley-VCH: Weinheim, 1988.

49. Stroppa, A.; Kresse, G. The Shortcomings of Semi-local and Hybrid Functionals: What We Can Learn from Surface Science Studies. *New J. Phys.* **2008**, *10*, 063020.

50. Albright, T.; Burdett, J.; Whangbo, M.-H. *Orbital Interactions in Chemistry*; John Wiley and Sons, Inc.: New York, 1985.

51. Fukui, K. The Role of Frontier Orbitals in Chemical Reactions (Nobel Lecture). *Angew. Chem., Int. Ed. Engl.* **1982**, *21*, 801–809.

52. Hoffmann, R. Building Bridges between Inorganic and Organic Chemistry (Nobel Lecture). *Angew. Chem., Int. Ed. Engl.* **1982**, *21*, 711–800.

53. Doye, J. P. K. Identifying Structural Patterns in Disordered Metal Clusters. *Phys. Rev. B* **2003**, *68*, 195418.

54. Marks, L. D. Experimental Studies of Small-Particle Structures. *Rep. Prog. Phys.* **1994**, *57*, 603–649.

55. Yacamán, M. J.; Ascencio, J. A.; Liu, H. B.; Gardea-Torresdey, J. Structure Shape and Stability of Nanometric Sized Particles. *J. Vac. Sci. Technol., B* **2001**, *19*, 1091–1103.

56. del Rosal, I.; Truflandier, L.; Poteau, R.; Gerber, I. C. A DFT Study of Spectroscopic and Thermodynamic Properties of Surfacic Hydrides on Ru(0001) Model Surface: The Influence of the Coordination Modes and the Coverage. *J. Phys. Chem. C* **2011**, *115*, 2169–2178.

57. van Santen, R. Symmetry Rules in Chemisorption. *J. Mol. Struct.* **1988**, *173*, 157–172.

58. Pan, C.; Pelzer, K.; Philippot, K.; Chaudret, B.; Dassenoy, F.; Lecante, P.; Casanove, M.-J. Ligand-Stabilized Ruthenium Nanoparticles: Synthesis, Organization, and Dynamics. *J. Am. Chem. Soc.* **2001**, *123*, 7584–7593.

59. Abild-Pedersen, F.; Greeley, J.; Studt, F.; Rossmeisl, J.; Munter, T. R.; Moses, P. G.; Skúlason, E.; Bligaard, T.; Nørskov, J. K. Scaling Properties of Adsorption Energies for Hydrogen-Containing Molecules on Transition-Metal Surfaces. *Phys. Rev. Lett.* **2007**, *99*, 016105.

60. Perdew, J. P.; Burke, K.; Ernzerhof, M. Generalized Gradient Approximation Made Simple. *Phys. Rev. Lett.* **1996**, *77*, 3865–3868.

61. Blöchl, P. Projector Augmented-Wave Method. *Phys. Rev. B* **1994**, *50*, 17953–17979.

62. Kresse, G.; Joubert, D. From Ultrasoft Pseudopotentials to the Projector Augmented-Wave Method. *Phys. Rev. B* **1999**, *59*, 1758–1775.

63. Kresse, G.; Fürthmuller, J. Efficient Iterative Schemes for *ab Initio* Total-Energy Calculations Using a Plane-Wave Basis Set. *Phys. Rev. B* **1996**, *54*, 11169–11186.

64. Kresse, G.; Fürthmuller, J. Efficiency of *ab Initio* Total Energy Calculations for Metals and Semiconductors Using a Plane-Wave Basis Set. *Comput. Mater. Sci.* **1996**, *6*, 15–50.

65. Monkhorst, H. J.; Pack, J. D. Special Points for Brillouin-Zone Integrations. *Phys. Rev. B* **1976**, *13*, 5188–5192.

66. Froemming, N. S.; Henkelman, G. Optimizing Core-Shell Nanoparticle Catalysts with a Genetic Algorithm. *J. Chem. Phys.* **2009**, *131*, 234103.